Ecological Engineering 127 (2019) 75–87

Contents lists available at ScienceDirect

Ecological Engineering

journal homepage: www.elsevier.com/locate/ecoleng

China's progress towards sustainable land degradation control: Insights from the northwest arid regions

Chong Jiang[a,b,c], Junguo Liu[a,b,*], Haiyan Zhang[d], Zhidong Zhang[a,b], Dewang Wang[e]

[a] Guangdong Provincial Key Laboratory of Soil and Groundwater Pollution Control, School of Environmental Science and Engineering, Southern University of Science and Technology, Shenzhen 518055, China
[b] State Environmental Protection Key Laboratory of Integrated Surface Water-Groundwater Pollution Control, School of Environmental Science and Engineering, Southern University of Science and Technology, Shenzhen 518055, China
[c] School of Water Resources and Hydropower Engineering, Wuhan University, Wuhan 430072, China
[d] Institute of Geographical Sciences and Natural Resources Research, Chinese Academy of Sciences, Beijing 100101, China
[e] Chinese Research Academy of Environmental Sciences, Beijing 100012, China

ARTICLE INFO

Keywords:
Wind erosion
Soil loss
Climate change
Ecological restoration
Constraint effect

ABSTRACT

Soil erosion is a widespread environmental problem, which threatens the environmental sustainability. The northwest arid region (NAR) in China is known as one of the most severe soil loss in the world that suffering from wind erosion. Based on the Revised Wind Erosion Equation (RWEQ), the spatio-temporal change of wind erosion was identified, and the underlying drivers and influencing factors of soil erosion process were investigated. In addition, the implications of constraint effects in soil erosion control were discussed. The results showed that the wind erosion from 1990 to 2013 was substantially lessened, and the government-aided desertification prevention and control programs, as well as increasing precipitation and decreasing wind speed might have contributed to these trends. The constraint line analyses indicated that the vegetation cover had nonlinear and threshold effects on soil erosion through constraining the water condition (precipitation). Specifically, when the precipitation is below the threshold (approximately 50–100 mm yr^{-1} in the NAR), the precipitation (water condition) is not sufficient to maintain a good vegetation cover (about 20–40%), therefore the vegetation cannot efficiently prevent wind erosion. However, once the precipitation exceeds this threshold, the vegetation's sand retention function will enhance and thereby reducing soil loss substantially. Vegetation cover has a lower and an upper threshold for controlling wind erosion. A plant cover lower than 10% does little to reduce wind velocity at the soil surface. The effect of vegetation on reducing wind erosion basically reaches the maximum when plant cover is 40% or above. The constraint effects of precipitation on vegetation cover in the arid region should be considered to improve the efficiency of afforestation and reforestation efforts aiming at mitigating and preventing soil loss.

1. Introduction

Soil is important for maintaining the normal operation of surface ecosystems (Pimental et al., 1995; Singer and Warkentin, 1996). In relation to the increasing effects of global warming and human disturbance, soil erosion has become one of the largest and most widespread environmental threats that greatly affect the sustainable development of social economies (Xu et al., 2013; Guo et al., 2012, 2018). Soil erosion negatively impact local ecology, leading to a deterioration in water quality, lowering effective levels of reservoir water, reducing crop productivity, and enabling flooding and habitat destruction (Shi et al., 2002; Xiao et al., 2017; Guo et al., 2018). More than 17.5% of the land area around the world is undergoing soil erosion by wind and water (Pimental et al., 1995). These areas are mainly distributed in the Eyre Lake and Murray Darling River regions of Australia, the Sahel region, Namib Desert, and Kalahari Desert in Africa, the Great Basin region in the western part of North America, the regions between the Andes and the Brazilian Plateau, and Central Asia (e.g., McIntosh, 1983; Teller and Lancaster, 1986; Knighton and Nanson, 1994; Jones and Blakey, 1997; Bourke and Pickup, 1999; Bullard and McTainsh, 2003). China is also one of the countries suffering the most severe soil erosion, with a total area simultaneously suffering soil erosion by wind and water of up to 3560×10^3 km^2 (MWRPRC, 2001; Wang et al., 2016a,b). In the northwestern China, large area of land usually suffers from

* Corresponding author at: School of Environmental Science and Engineering, Southern University of Science and Technology, Shenzhen 518055, China.
E-mail address: junguo.liu@gmail.com (J. Liu).

https://doi.org/10.1016/j.ecoleng.2018.11.014
Received 27 August 2018; Received in revised form 30 October 2018; Accepted 10 November 2018
Available online 19 November 2018
0925-8574/ © 2018 Elsevier B.V. All rights reserved.

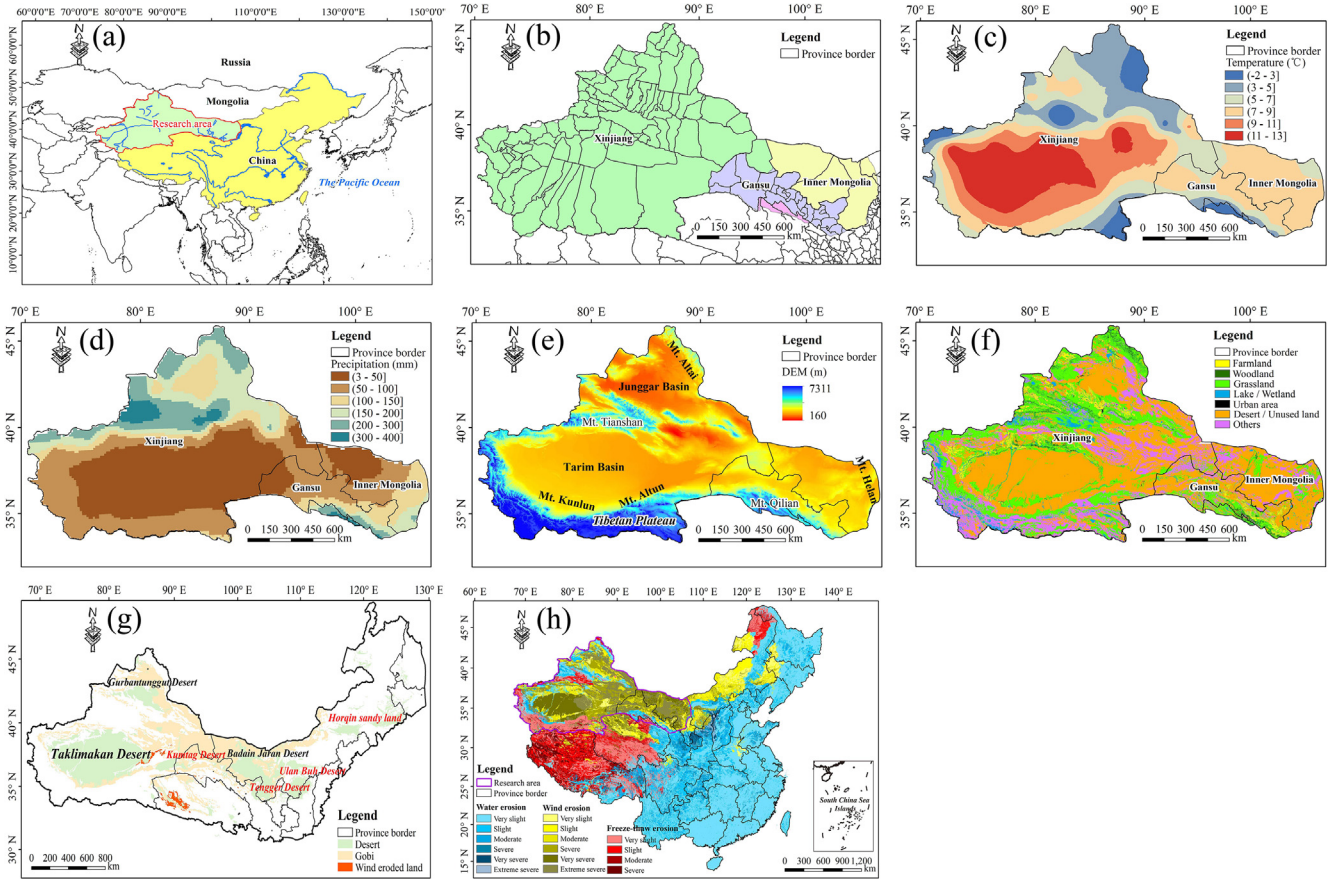

Fig. 1. (a) Location of the northwest arid region (NAR) and general description of geographical information, (b) Administrative divisions, (c) Spatial distribution of annual mean temperature, (d) Spatial distribution of annual precipitation, (e) Digital Elevation Model (DEM), (f) Land use/cover map (ecosystem types), (g) Distribution of desert, Gobi, and wind eroded land, and (h) Distribution of soil erosion types.

complex soil erosion by wind and water, which is a threat to sustainable agriculture and environmental quality (Du et al., 2015, 2016; Guo et al., 2018).

The process of soil erosion is mainly controlled by natural and human factors such as soil texture, soil physical and chemical composition, climate condition (precipitation and temperature), terrain (slope, aspect, and shape), ground cover (vegetation cover and land cover), and interactions between them (Alexander et al., 2017; Li et al., 2017; Wei et al., 2017). Substantial efforts have been made to develop quantitative assessment models of soil erosion, and those developed mainly belong to two categories, either on-site measurements that are often applied in small-scale regional or point experiments or off-site quantification models, which can be used to evaluate the erosion intensity of zones on a large scale (Tamene et al., 2006; Xu et al., 2013; Ganasri and Ramesh, 2016). Models are developed to quantify soil erosion such as the universal soil loss equation (USLE) (Renard et al., 1997; Mattheus and Norton, 2015), the water erosion prediction project (WEPP) (Ascough et al., 1997; Baigorria and Romero, 2007), the European soil erosion model (EUROSEM) (Morgan et al., 1998; Naser et al., 2016), and the Erosion for Agricultural Management system (CREAMS) (Knisel, 1980; Vanwalleghem et al., 2017). However, studies of wind erosion assessment are relatively rare, and the assessment methods are mainly involved some intrinsic (mainly are soil characters) and extrinsic factors (i.e., topography, meteorological conditions, etc.) (Hoffmann et al., 2011); and the models are essentially the Revised Wind Erosion Equation (RWEQ) or the Wind Erosion Prediction System (WEPS) (Coen et al., 2004; Hagen, 2004; Mendez and Buschiazzo, 2010; Du et al., 2015). Basically, this study selected the RWEQ to assess and map the wind erosion in the northwest arid region (NAR). This is because the model has multiple advantages, such as simple modeling processes, fewer input parameters, and easily integrates with GIS database.

The northwestern China is one of the most severely eroded regions by wind in the world (Tang, 2004), with the average erosion modulus of 5000–10000 t km^{-2}. In the northwest China, desert areas widely distribute, which occupy approximately 13% of the country's total land area, and they are major sources of Asian sandstorm (Song, 2004). Because of severe soil erosion, a mass of sediment is fed into the Yellow River by winds and tributary inflows and has silted up the main channel (Zhao et al., 2013, 2014). In order to improve environment and combat desertification, the Chinese central government has implemented several desertification prevention and control programs including the Grain for Green Program (GFGP; Feng et al., 2003; Wang et al., 2007), the Green Great Wall Program (GGWP; Fang et al., 2001), and the Natural Forest Conservation Program (NFCP; Zhang et al., 2000). Among them, the GGWP is arguably one of the most aggressive programs of the 20th century (Parungo et al., 1994; Yin and Yin, 2010; Zhang et al., 2016). After the implementation of the GGWP, weather it brought about the desired effect of lessening wind erosion? Some authors consider the GGWP to have been successful, pointing to the fact that the forest cover rate has increased from 5.1% in 1978 to 9.0% in 2001 (Zhu et al., 2004), and that vegetation conditions have improved (Duan et al., 2011; Zhang et al., 2016). Both of these factors control desertification and may reduce wind erosion intensity. Conversely, other studies concluded that the GGWP's effectiveness at controlling sandstorms should be questioned (Wang et al., 2010).

Generally, wind erosion is related to (semi-) arid region, and water erosion usually occurs in humid zone. However, in some arid or semi-

arid regions (e.g., NAR), both erosion processes contribute significantly to soil erosion and sometimes occur simultaneously. An assessment of soil erosion that focused on only one stress might therefore provide incomplete information for soil erosion control. In the NAR, so far, studies of the complete assessment of wind are very few, and the underlying drivers for soil erosion change are still not fully understood. In addition, the complex interactions between soil erosion and influencing factors (i.e., land cover, soil type, climate condition, vegetation cover) have not been reported thoroughly. In light of above limitations and deficiencies, the objectives of this study are (1) to quantify and map the soil loss by wind based on RWEQ model in consideration of the regional terrain and geographical conditions; (2) to investigate the roles of climate variability and desertification prevention and control program in soil erosion' spatial pattern and temporal change; (3) to enrich the understanding of the relationship between soil erosion and influencing factors, in particular for vegetation cover and precipitation, by applying a new perspective concerning the constraint effects; and (4) finally discuss the implications of the constraint effects in soil erosion control. The results are expected to provide an important reference for estimating soil erosion in arid regions, particularly in the NAR, and then contribute to the control and prevention of soil erosion.

2. Research area descriptions

The northwest arid regions (NAR) is located in the hinterland of the Eurasian continent (between 73.5°–107.2°E and 34.4°–49.2°N), which is about 2.5 million km^2, accounting for over 25% of the territory of China (Fig. 1(a)). The NAR mainly covers three administrative regions including Xinjiang Uygur Autonomous Region, the Midwest Inner Mongolia Autonomous Region, and the main body of Gansu province (Fig. 1(b)). The NAR is far from the sea, belongs to a temperate and warm temperate arid region with a typical continental dry climate, and is one of the most arid areas in the world. The spatial patterns of annual mean temperature and annual precipitation are consistent with topography (Fig. 1(c and d)), which means the mountain areas (i.e., Mount Tianshan, Mount Altai, and Mount Qilian) have more precipitation and lower temperature, while the basin areas (Junggar Basin and Tarim Basin) are characterized by warm and arid climate. The topography is relatively complicated which stretches from the Mount Kunlun in the west with elevation of higher than 7300 m to Mount Helan in the east (lower than 1000 m; Fig. 1(e)). The northern boundary is Mount Altai, and the southern part reaches Tibetan Plateau. The research area belongs to typical arid eco-fragile area due to water resources shortage, widespread desertification, and sparse vegetation. The main land use/cover types include desert/unused land and grassland, while the other types only account for a very small part (Fig. 1(f)). The main deserts from west to east are Taklimakan Desert, Gurbantunggut Desert, Kumtag Desert, and Badain Jaran Desert (Fig. 1(g)). In particular for the Taklimakan Desert, it is the largest desert in China, which is also the second largest one around the world. Due to the arid and windy climate condition and easily erodible soil types (i.e., eolian sandy soil, chernozem, kastanozems, brown soil and sierozem), this area experiences severe wind erosion (Fig. 1(h)). In order to improve environment and combat desertification, the central government has implemented several desertification prevention and control programs including GFGP, GGWP and NFCP, and the total area of multiple programs in the Xinjiang during 2000–2010 reaches approximately 0.8 million ha (SFA, 2010).

3. Data and methods

3.1. Data sources

In this study, multi-source datasets were collected and used for the soil erosion assessment, the data description, type, resolution, source, and related reference could be found in Supplementary Table 1. The climate data were rated as good quality, and the overall data missing ratio was smaller than 5%. Missing observation records in climate data were estimated from the average value in the same year observed at the neighboring stations. All climate datasets were spatially interpolated to a 1 km spatial resolution before they were input into the assessment models. Annual and seasonal average values of climatic variables were then calculated from the daily measurements. Regional average levels of climatic variables were calculated by mean values of stations within the study area (Jiang et al., 2017). Soil data derive from China's second national soil survey, which is available at Cold and Arid Regions Sciences Data Center (http://westdc.westgis.ac.cn/data/). This information includes soil types, particle-size distribution, soil organic matter content, and soil depth at a scale of 1:1 million. Topographic data were derived from NASA's Shuttle Radar Topography Mission (http://www:jpl.nasa.gov/srtm) digital elevation model (DEM), with a horizontal resolution of 30 m. This study used this information to reflect topography change and climate data interpolation. The land use datasets (Liu et al., 2005, 2014) in 1990, 2000, and 2015 were derived from the Landsat TM/ETM data at a spatial resolution of 1 km and are available from the Chinese Academy of Sciences' Data Center for Resources and Environmental Sciences (http://www.resdc.cn/). Based on ground truth data, the overall accuracy of the land use/cover map is higher than 90% for the three periods. Because the normalized difference vegetation index (NDVI) is a good indicator for vegetation cover detection, this study used the Moderate Resolution Imaging Spectroradiometer (MODIS) time series NDVI dataset (MOD13Q1 product) from 2000 to 2013, which was obtained from the NASA EOS DATA Gateway (https://wist.echo.nasa.gov/api). The spatial resolution was 250 m, and the time interval was 16 days. Because cloud cover, atmospheric conditions, and ice and snow cover can affect MODIS products, this study used the asymmetric Gaussian filter during data pre-processing to reduce noise and improve data quality, which was based upon TIMESAT 2.3 software (http://web.nateko.lu.se/timesat/timesat.asp). To further eliminate noise, we compiled resultant 16-day MODIS NDVI data into monthly NDVI data by applying maximum value composites (MVC) (He et al., 2015; Qu et al., 2015) to the two NDVI images of each month. In addition, the long term NDVI dataset generated from NOAA's Advanced Very High Resolution Radiometer (AVHRR) with a resolution of 8 km for 1982–2013 were also used to detect the vegetation cover change in the past three decades.

3.2. Quantifying soil loss by wind erosion

In this study, the Revised Wind Erosion Equation (RWEQ) model issued by United States Department of Agriculture (USDA) (Fryrear et al., 1998) was used to simulate the wind erosion modulus in the NAR. The RWEQ model is an empirical-based model developed by Fryrear et al. (1998) in order to estimate soil loss from arable land in United State. This model not only is a good applicable methodology for the prediction of wind erosion at a field scale, but also provides information on erosion rates on regional scale (Fryrear et al., 1998). The RWEQ model has a simple structure that make it easier to scale up using GIS technologies than the other models with more parameters and complex structure, and it depends several factors multiplying to get the aeolian sediment maximum transport capacity (Cantón et al., 2011; Youssef et al., 2012).

The RWEQ model estimates wind erosion and sediment transport by wind between the soil surface and a height of 2 m for specified periods based on a single event. The sediment maximum transport capacity, Q_{max} (kg m^{-1}), can be calculated as:

$$Q = \mu_q \times WF \times EF \times SCF \times K \times COG \quad (1)$$

where μ_q is a dimensionless parameter to adjust the sediment maximum transport capacity, Fryrear et al. (1998) suggested it was 109.8 according to the experimental data in Great Plains of the U.S., and we set

it is an adjustable parameters to adjust the calculate result in this study; *WF* is a weather factor (kg m^{-1}); *EF* is the soil erodible fraction (%); *SCF* is the crust factor, dimensionless; *K* is the roughness factor, dimensionless; and *COG* is the combined crop factor, dimensionless.

The weather factor (*WF*) can be calculated as:

$$WF = \frac{SW \times SD \times \sum_{i=1}^{N} u_2(u_2 - u_t) \times N_d \times \rho}{Ng} \quad (2)$$

where u_2 is the wind speed at a height of 2 m (m s^{-1}), and it can be converted from wind speed observed at standard anemometer heights by the 1/7 power expression method (Fryrear et al., 1998); u_t is the threshold wind speed at a height of 2 m (m s^{-1}), given that Liu et al. (1998) suggested that the threshold wind speed for the arable lands in north-central parts of China is 6 m s^{-1} according to their wind tunnel experiments; N_d is the number of days in period (usually 15 days); *N* is the observation frequency of wind speeds during a period, usually 500, and can be calculated by the sub-daily wind speed calculator (Skidmore and Tatarko, 1990; Du et al., 2014a,b); *g* is gravitational acceleration (m s^{-2}); *SD* is a snow cover factor, dimensionless, because the precipitation in winter is very less, the snow cover is very rare. Hereby, the effect of snow cover factor can be ignored in the NAR, and *SD* is equal to 1; and *SW* is a soil wetness factor, dimensionless, and which can be calculated as:

$$SW = \frac{ET_p - (R + I)\left(R_d/N_d\right)}{ET_p} \quad (3)$$

where ET_p is the potential relative evapotranspiration (mm), which can be used by a method proposed by Samani and Pessarakli (1986); $R + I$ is precipitation and irrigation (mm); R_d is the number of precipitation and irrigation days. The precipitation and the number of precipitation days were obtained from meteorological data. Every weather factor *WF* was calculated on the basis of 500 wind speed values during 1–15 days, 500 being the minimum number of wind speed values needed to express the wind speed distribution in a given place.

The soil erodible fraction (*EF*) depends on soil texture and can be calculated as:

$$EF = \frac{\mu EF + 0.31Sa + 0.17Si + 0.33Sa/Si - 2.59OM - 0.95CaCO_3}{100} \quad (4)$$

where μEF is a calibrated parameter for soil erodible fraction (%); *Sa* is the sand content (%); *Si* is the silt content (%); *OM* is the organic matter content (%); and $CaCO_3$ is the calcium carbonate content (%).

The soil crust factor (*SCF*) is determined from the abrasion coefficient on clay and organic matter content and can be calculated as:

$$SCF = \frac{1}{1 + 0.0066Cl^2 + 0.021OM^2} \quad (5)$$

where *Cl* is the clay content (%). In this study, it was assumed that the soil crust factors do not change over time. The factors of *EF* and *SCF* were calculated by the 1:1 million soil map, which included many soil physicochemical properties.

The soil roughness factor (*K*) is related to chain random roughness C_{rr} (cm) and soil ridge roughness K_r (cm), and it can be expressed as:

$$K = e(1.86K_{r\ \mathrm{mod}} - 2.41K_{r\ \mathrm{mod}}^{0.934} - 0.124C_{rr}) \quad (6)$$

$$K_r = \frac{RH^2}{RS} \quad (7)$$

$$R_c = 1 - 0.00032A - 0.000349A^2 + 0.0000258A^3 \quad (8)$$

where *RH* and *RS* are the height and spacing respectively of ridges in the arable lands (cm), and were obtained according to Du et al. (2015, 2016); K_{rmod} is a modified roughness factor which is the product of the ridge roughness K_r and the rotation coefficient R_c; and *A* is the wind angle to the ridges (0° if perpendicular, 90° if parallel). The chain random roughness C_{rr} and soil ridge roughness K_r were obtained through field observation in some typical arable lands (Du et al., 2015, 2016).

The combined crop factor *COG* includes three factors: flat residues SLR_f, standing residues SLR_s, and crop canopy SLR_c. In the RWEQ, the flat residues are anything lying on the soil surface. According to the concept of flat residues, it was recognized that flat residues in this case are crushed straw. However, after harvest, crop straw is normally used as cattle fodder in the northwest of China (Du et al., 2016). Therefore, the impact of flat residues on wind erosion can be ignored to simplify the model, and the flat-residues factor can be assumed to be one.

The standing residues, SLR_s, were summarized into a soil-loss ratio coefficient that reflects the silhouette of standing material and can be calculated as:

$$SLR_s = e^{-0.0344SA^{0.6413}} \quad (9)$$

where *SA* is the silhouette area, which is computed by multiplying the number of standing stalks in 1 m^2 by the average diameter and the stalk height.

Emerging crop seedlings and subsequently larger plants provide a partial canopy cover over the soil. To convert the influence of crop canopy to soil ratio, the RWEQ model uses a computer based method (Fryrear et al., 1998):

$$SLR_c = e^{-5.614cc^{0.7366}} \quad (10)$$

where *cc* is the fraction of the soil surface covered by crop canopy and is calculated by NDVI values based on field observation (Du et al., 2014a,b).

3.3. Validation of model estimated erosion modulus

In order to check the accuracy of model estimated erosion modulus in the NAR, the erosion moduli obtained by ^{137}Cs observation were collected from related literature to do a comparison. The ^{137}Cs method provides a relatively simple means of assembling information on long-term rates and patterns of soil erosion, which can be used to test and validate the performance of soil erosion models (Walling et al., 2003). In this study, the validation was based on a comparison between soil loss measured by ^{137}Cs and that predicted from the RWEQ model. As shown in Supplementary Fig. 1, a significant relationship ($P < 0.0001$) between the erosion rate determined by ^{137}Cs measurement and the model estimated result was found. The coefficient of determination (R^2) was 0.85, and the deviation of the regression coefficient might be attributed to the spatial heterogeneity at 1 km spatial resolution because of the mosaic of different vegetation and topography patterns. However, this finding showed that the model could provide relatively accurate estimated result.

3.4. Statistical analysis

We used linear regression to analyze the temporal change in average soil erosion at the sub-zone level. In addition, we examined the major drivers of soil erosion using constraint line analysis (Thomson et al., 1996; Guo et al., 1998). In bivariate scatter grams, data points sometimes show clouds bounded by an informative edge, implying that the independent variable may act as a limiting factor constraining the response of the dependent variable (constraint effect). In this case, constraint line analysis has been suggested in lieu of traditional correlation and regression methods (Wang et al., 2016a,b; Hao et al., 2017). This was the case for the scatter grams of soil erosion versus vegetation cover and precipitation. Thus, we quantified the constraint (or limiting) effects of vegetation cover and precipitation on soil erosion using the constraint line method introduced by Wang et al. (2016a,b) and Hao et al. (2017). Specifically, we mapped the scatter plots and constraint lines of wind erosion modulus versus precipitation (vegetation cover) for the sub-zones of NAR at pixel scale, the results about the

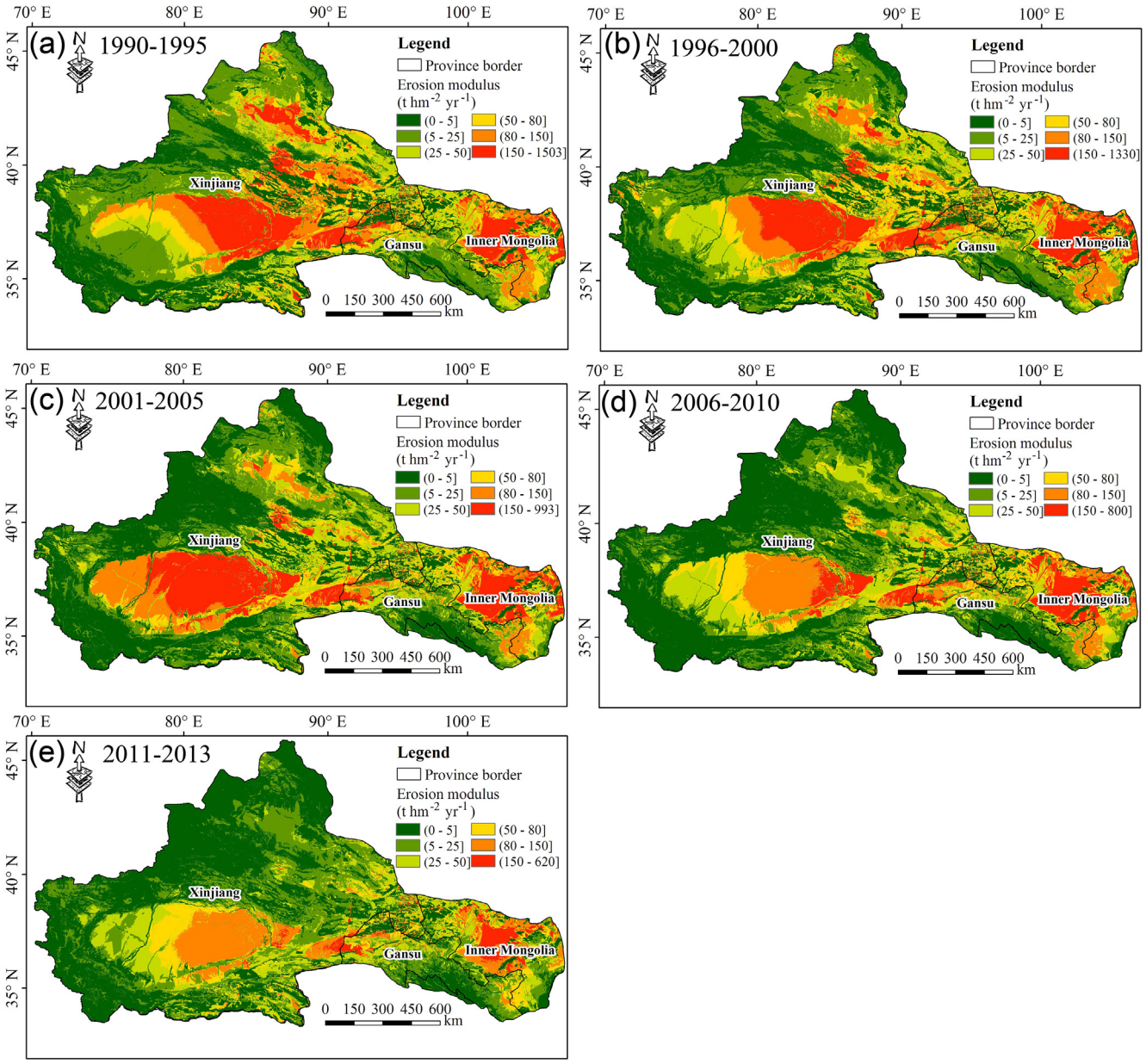

Fig. 2. Spatial distributions of period average soil erosion modulus in (a) 1990–1995, (b) 1996–2000, (c) 2000–2005, (d) 2006–2010, and (e) 2011–2013.

relationship between soil erosion and precipitation (vegetation cover) will be introduced in Sections 4.4 & 4.5.

4. Results and discussions

4.1. Spatial pattern and temporal change of wind erosion

The spatial patterns of wind erosion in the NAR presented clearly spatial heterogeneity, see Figs. 2 and 3. As shown in Fig. 2(a–e), the relatively high wind erosion intensity in multiple periods (1990–1995, 1996–2000, 2001–2005, 2006–2010, and 2011–2013) was located mostly in several large deserts (e.g., Taklimakan Desert, Gurbantunggut Desert, Kumtag Desert, and Badain Jaran Desert). The altitude zones of 0–700 m, 700–1400 m, 1400–2000 m presented the highest erosion intensity (larger than 40 t ha^{-1} yr^{-1} during 1990–1998; Fig. 3(a)). Meanwhile, the low values of erosion moduli were mainly found in woodland and grassland ecosystems (e.g., central part of Xinjiang and southern Gansu) and mountain areas (e.g., Mount Altai, Mount Tianshan, Mount Altun, Mount Kunlun, and Mount Tianshan), the zonal statistics see Fig. 3(b). In the mountain areas, the main land covers are woodland and grassland, whose vegetation cover is relatively high comparing with desert. In addition, the precipitation in the mountain area is relatively sufficient, thus the wind erosion is not serious. However, in the southern Xinjiang and Inner Mongolia, the topography is gentle and the dominant land covers are desert and unused land, thus the arid climate is much easier to induce severe wind erosion.

The temporal change of wind erosion from 1990 to 2013 was shown in Fig. 4. As shown in Fig. 4(a), the wind erosion moduli declined substantially in all altitude zones, in particular for 0–700 m and 700–1400 m. The similar declining trends were also detected in different ecosystem types, see Fig. 4(b). In the comparison between 1990 and 2013, the erosion modulus in the Xinjiang decreased from 55.5 t ha^{-1} yr^{-1} in 1990 to 19.3 t ha^{-1} yr^{-1} in 2013, and the Gansu also dropped almost by half (from 42.8 t ha^{-1} yr^{-1} in 1990 to 27.6 t ha^{-1} yr^{-1} in 2013). The declining trend in wind erosion generally corresponds to recent studies reporting on the wind erosion change in the NAR and neighboring areas, for instance the watershed of the Ningxia-Inner Mongolia Reach of the Yellow River (Du et al., 2015,

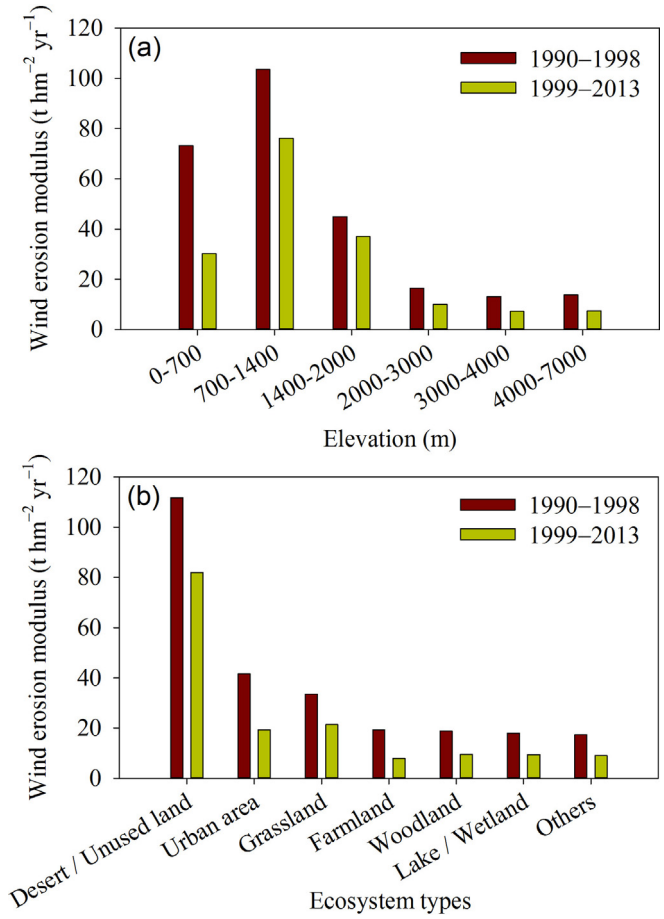

Fig. 3. The comparison of zonal average wind erosion moduli between 1990 and 1998 and 1999–2013 in sub-zones: (a) elevation belts and (b) ecosystem types.

2016), the Xilingol League of Inner Mongolia (Gong et al., 2014a,b), and northern China (Gong et al., 2014c).

4.2. The underlying drivers for wind erosion change

4.2.1. Climatic drivers

Overall, annual mean wind speed decreased significantly by 0.10 m s^{-1} decade^{-1} ($p < 0.01$) in the NAR during the 1960–1989, and the declining trend continued from 1990 to 2013 (-0.10 m s^{-1} decade^{-1}, $p < 0.001$, Fig. 5(a)). In terms of the spatial distribution as shown in Fig. 6(a), the wind speed declined consistently almost in entire area, and the largest declining trends ($-0.4 \sim -0.3$ m s^{-1} decade^{-1}) lied in the northern area. Only very few stations around Mount Tianshan and Mount Qilian presented increasing trends (0–0.2 m s^{-1} decade^{-1}). For the annual precipitation as shown in Figs. 5(b) & 6(b), it fluctuated largely from 1960 to 2013, and the change trends for both periods of 1960–1989 and 1990–2013 were not significantly. As shown in Figs. 5(c) & 6(c), during 1982–1989, the annual growing season NDVI for the entire NAR increased by 0.002 yr^{-1} ($p > 0.05$), while it fluctuated largely from 1990 to 2013 with no significant trend detected. The wind speed and wind erosion modulus also presented a corresponding relationship (Figs. 4(a and b) & 5(a)), thus, as the erosion force, the wind speed increment (decrement) aggravated (lessened) the wind erosion. Wind erosion is often manifested in the form of sandstorm, as shown in Figs. 5(a, c) & 6(a, c), decreasing wind speed since the early-1970s has reduced frequency of sandstorm event significantly. Tan and Li (2015) concluded that GGWP greatly improved the vegetation cover and effectively reduced sandstorm intensity in northern China. In this study, although the vegetation restoration in the NAR was not significant (Fig. 5(c)), we also found the declining sandstorm event frequency, which was basically similar to the declining trend in the GGWR (Tan and Li, 2015).

4.2.2. Sand prevention and control programs

In order to contain the desertification in the NAR, in particular around the southern Xinjiang (i.e., Taklimakan Desert), the central and local government initiated a series of large scale desertification prevention and control programs since 1978 (He et al., 2015). Taking the Xinjiang as an example, the GGWP totally involved 3.4×10^6 ha from 1978 to 2008, which improved the vegetation cover by 1.91% (SFA, 2010). As shown in Fig. 7, the vegetation restoration (positive NDVI trend) from 1990 to 2013 was significant in mountain areas (i.e., Mount Tianshan, Mount Kunlun, Mount Qilian) at annual and seasonal scales, while the other areas, where deserts located in, experienced vegetation degradation (negative NDVI trend). Due to the mountain areas with positive NDVI trend only accounted for less than 35%, therefore the NDVI change for the entire NAR presented large fluctuation, and no significant trend was detected (Fig. 5(c)). In terms of the GFGP, it totally involved 626×10^3 ha from 1999 to 2010, which mainly included two ecosystem conversion types, i.e., farmland to woodland and farmland to grassland (SFA, 2010).

In the comparison between 1990 and 2000 (Fig. 8(a, b)), large areas of grassland, woodland, and desert/unused land were converted into farmland. Specifically, the total transfer areas in the Xinjiang were grassland to farmland (11804.7 km^2), woodland to farmland (1133.1 km^2), and desert/unused land to farmland (3662.8 km^2). Meanwhile, in the Gansu Province, the transfer areas were grassland to farmland (22389.3 km^2), woodland to farmland (2858.1 km^2), and desert/unused land to farmland (1685.3 km^2). During the period 2000 to 2015, in spite of the implementation of the GFGP, the area of cropland in the Xinjiang substantially increased. The cause is that the central government considers the cropland expansion in the northwest China as an offset of the cropland loss in eastern China induced by rapid urbanization (Liu et al., 2014). In the comparison between 2000 and 2015 (Fig. 8(c, d)), farmland expansion and woodland, grassland, and desert/unused land shrinkages were identified in three sub-zones, which was attributed to the rapidly increasing food demand (Liu et al., 2014). A large area of other land use/cover types (i.e., woodland, grassland, and desert/unused land) was replaced by farmland. For instance, the transfer areas from grassland to farmland and from desert/unused land to farmland in the Xinjiang were 12213.9 km^2 and 6496.7 km^2, respectively. In addition, large areas of desertification prevention and control programs have been implemented in the NAR since late 1970s, in particular after 1999, which included the grass pane, afforestation, and reforestation, the typical prevention and control projects were shown in Fig. 9. Therefore, we conclude that the desertification prevention and control programs play an important role in wind erosion reduction and desertification control.

4.3. Influences of land cover and soil type on soil erosion

The RWEQ model clearly show that several factors influence soil erosion. These factors include vegetation cover (the key resistance), weather factor (the key driving force), land cover types (influencing soil surface roughness, soil particles, and the development of wind profiles), and soil physical properties (determining soil erodibility or resistance to erosion). Below we briefly discuss how these factors affect soil erosion.

Change in land use types, as a controllable factor, has significant relationships with change of the soil erosion intensity (Guo et al., 2012). Determining the cause of land use changes on changes in the soil erosion intensity can thus provide important decision supports for use in compiling soil erosion prevention and governance strategies (Jiang et al., 2014). Land use/cover in the NAR has changed dramatically since 1990 because of the policy of returning farmland to forest and grassland

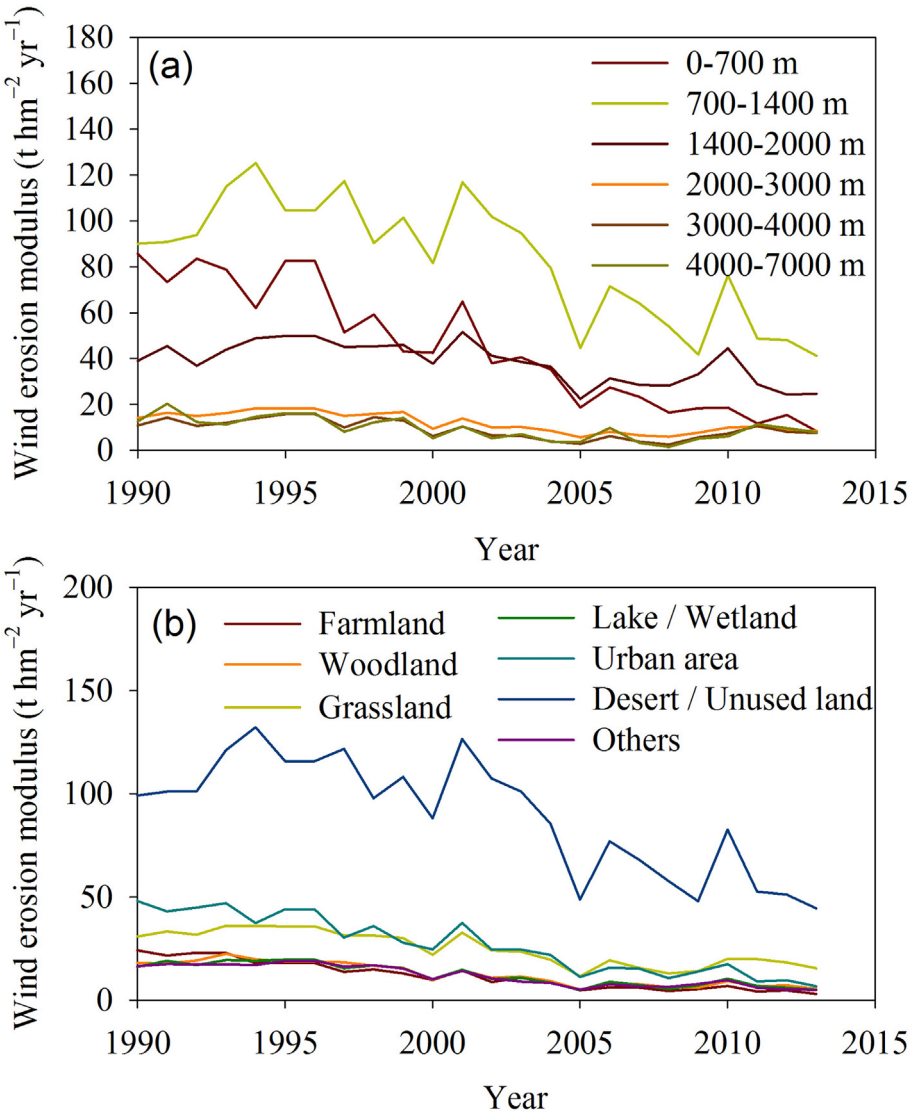

Fig. 4. The temporal changes of zonal average wind erosion moduli from 1990 to 2013 in sub-zones: (a) elevation belts and (b) ecosystem types.

(i.e., GGWP and GFGP, see Fig. 8). Although the wind erosion intensity is jointly influenced by land use change and wind speed variability, the desertification prevention and control can definitely shift the soil erosion (degradation) trend (Gong et al., 2014a,b,c; Zhao et al., 2017). In order to clarify the impacts of land use changes on wind erosion, we specifically investigated the soil erosion intensity change in different land use types (ecosystem types). In the comparison of 1990–1998 and 1999–2013, the zonal averaged wind erosion moduli in the desert and unused land were much larger than other types (Fig. 3(b)). During 1990–2013, the wind speed presented significantly decreasing trend (Fig. 5(a)), thereby the wind erosion moduli for seven ecosystems, in particular for the desert and grassland, showed declining trends (Fig. 4(b)).

Land cover type and soil property also contribute to the spatial pattern of wind erosion in the NAR. Soil types vary in texture, chemistry and organic matter content which influence soil particle size and weight, and their ability to retain moisture and form crust (Zhou et al., 2016; Tang et al., 2018; Zhang et al., 2018). All of above factors are important for determining soil erodibility (Rezaeiet al., 2016). Soil physical and chemical characteristics vary greatly between different land use/covers such as grassland and cropland (Rezaeiet al., 2016). Taking the Badain Jaran Desert and Taklimakan Desert as an example, soil loss due to wind erosion was much greater than other regions (Fig. 2(a–e)). Desert and unused land are covered mostly by the aeolian sandy soil, which are more vulnerable to wind erosion. This is an important reason why the Badain Jaran Desert and Taklimakan Desert experienced more severe wind erosion.

Tang et al. (2018) investigated the mechanism influencing variations in the soil infiltration capacity after vegetation restoration. They found that vegetation restoration effectively improved the soil infiltration capacity, which is closely related to the erosion force (runoff), and this improvement further reduced water erosion. Furthermore, Zhou et al. (2016) systematically analysed the interactive effects of precipitation and vegetation on soil erosion under different restored vegetation covers in the Loess Plateau, China, and they concluded that a vegetation restoration mode with a high canopy structure heterogeneity was more effective for controlling soil erosion. Besides, Zhang et al. (2018) concluded that long-term afforestation significantly improved the fertility of abandoned farmland and resulted in significant increases in the proportion of macro-aggregates, organic matter content and total nitrogen content, all of which significantly enhanced the soil's resistance to erosion.

4.4. Relationship between climate condition and wind erosion

Wind speed and precipitation (soil moisture condition) are the main

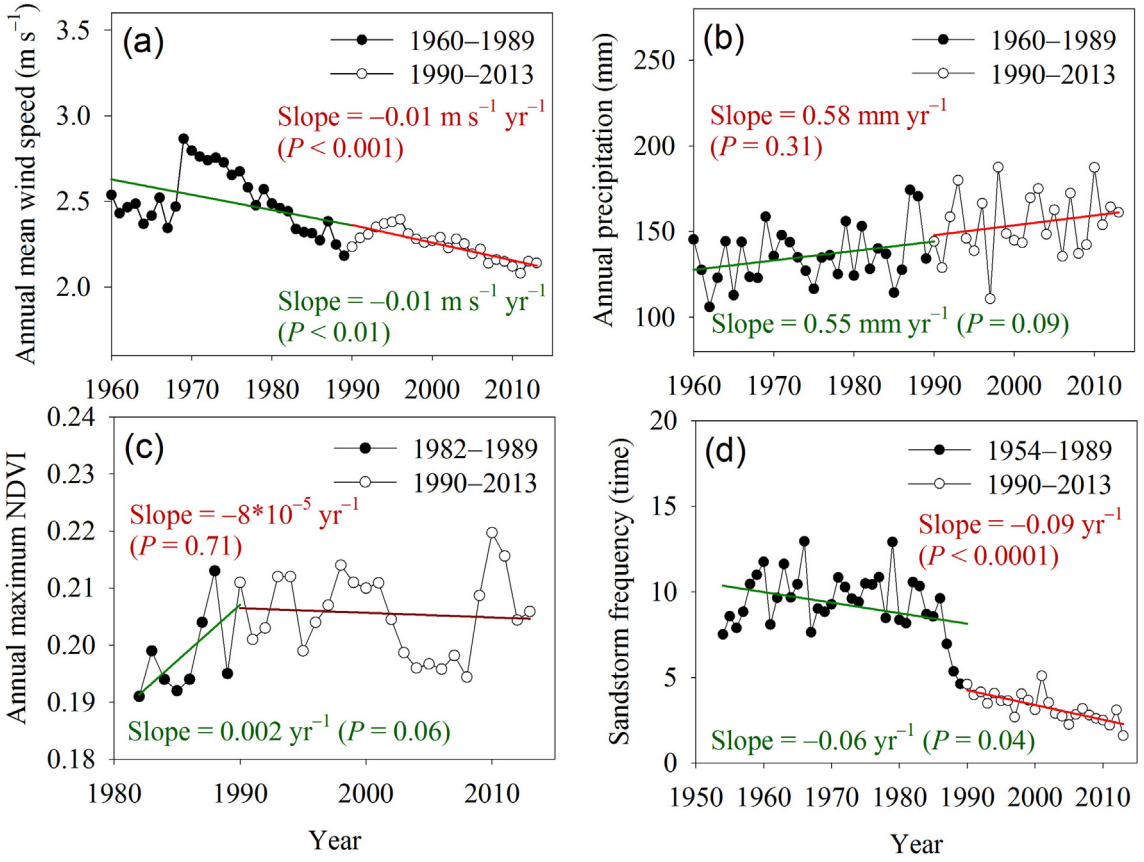
(a)
1960–1989
1990–2013
Slope = –0.01 m s^{-1} yr^{-1} (P < 0.001)
Slope = –0.01 m s^{-1} yr^{-1} (P < 0.01)
Annual mean wind speed (m s^{-1})
(b)
Slope = 0.58 mm yr^{-1} (P = 0.31)
Slope = 0.55 mm yr^{-1} (P = 0.09)
Annual precipitation (mm)
(c)
1982–1989
Slope = –8*10^{-5} yr^{-1} (P = 0.71)
Slope = 0.002 yr^{-1} (P = 0.06)
Annual maximum NDVI
(d)
1954–1989
Slope = –0.09 yr^{-1} (P < 0.0001)
Slope = –0.06 yr^{-1} (P = 0.04)
Sandstorm frequency (time)
Year
Year

Fig. 5. Temporal changes in (a) annual mean wind speed and (b) annual precipitation of the entire NAR during 1960–2013; (c–d) are annual growing season NDVI from 1982 to 2013 and sandstorm frequency between 1954 and 2013, respectively.

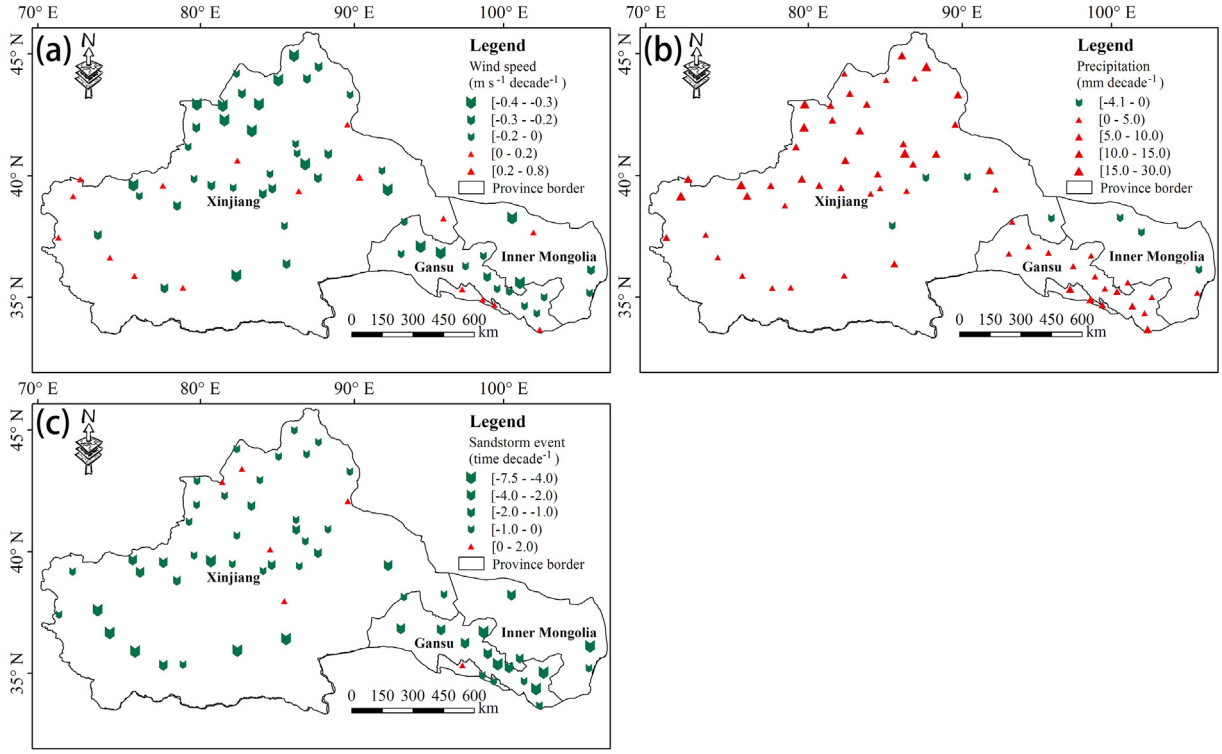

Fig. 6. Spatial distributions of trend slopes in (a) annual mean wind speed (1960–2013), (b) annual precipitation (1960–2013), and (c) sandstorm frequency (1954–2013).

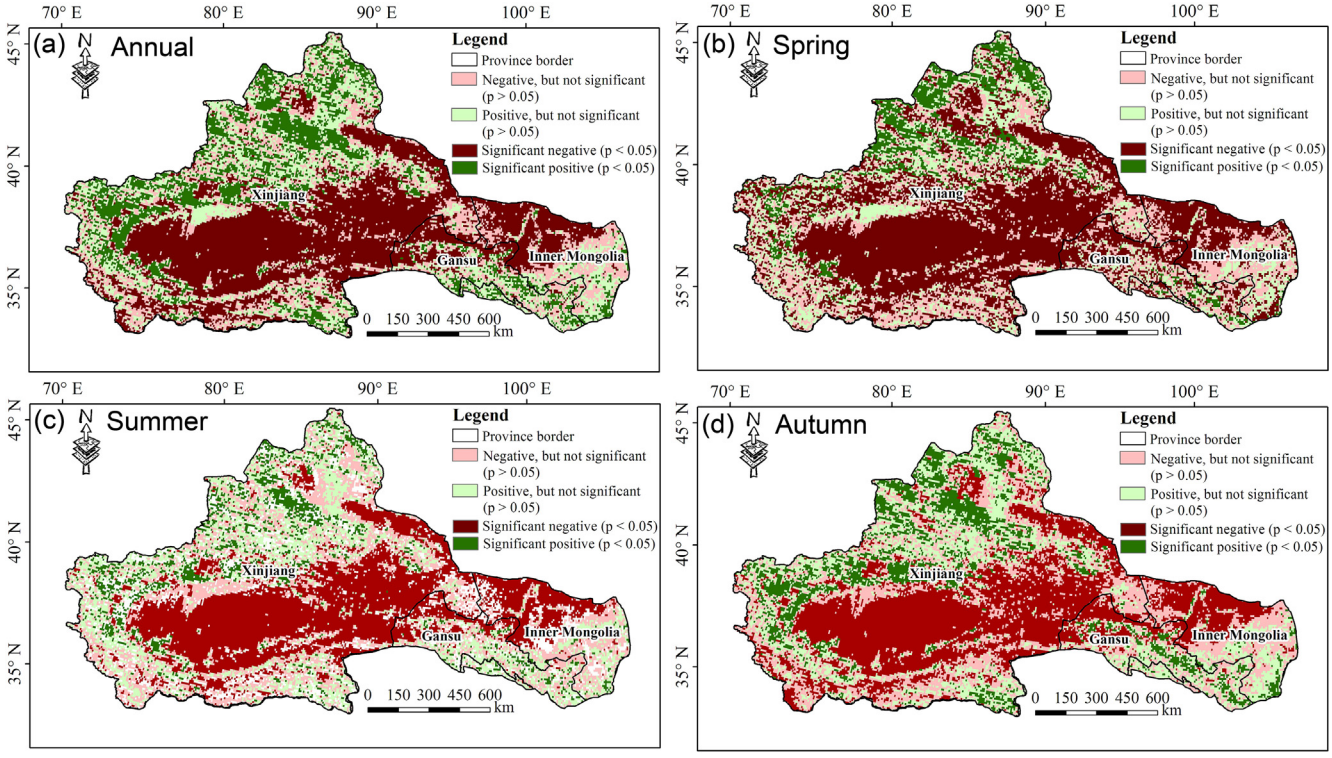

Fig. 7. Spatial distributions of annual growing season NDVI changes during 1990–2013: (a) annual scale, (b) spring, (c) summer, and (d) autumn.

factors influencing the sediment transport induced by wind erosion. For the wind erosion, it is a comprehensively influenced effect of several weather factors (i.e., precipitation, temperature, and wind speed; Zhao et al., 2017). The interaction of strong wind with dry, loose soil surface can cause serious erosion (Shao, 2008). Precipitation and temperature have important effects on soil erodibility (McKenna Neuman, 2003). Below we specifically discuss how these factors affected soil erosion.

In the Fig. 10(a–c), the scatter plots of soil erosion modulus against

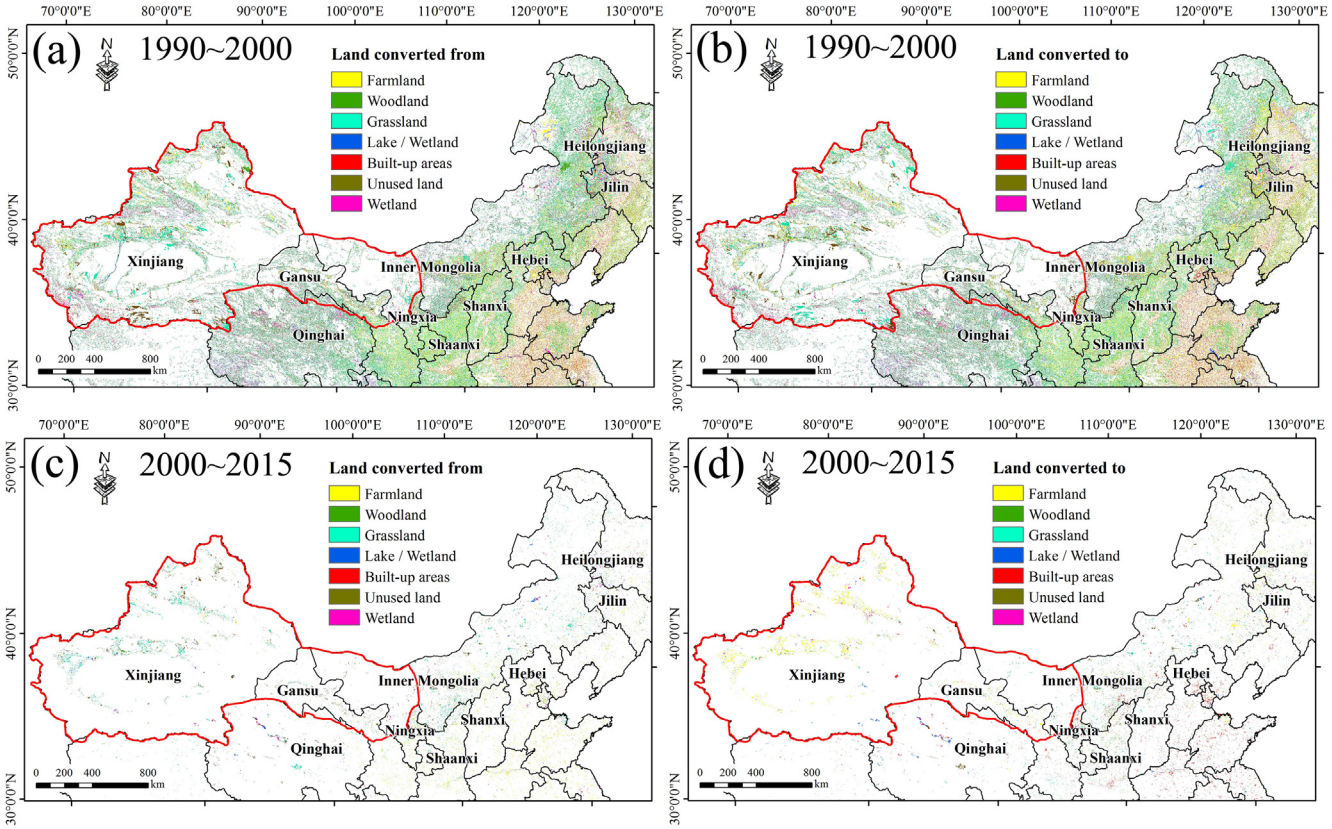

Fig. 8. Land use/cover conversions in the NAR and neighboring areas during the periods of (a–b) 1990–2000 and (c–d) 2000–2015, respectively.

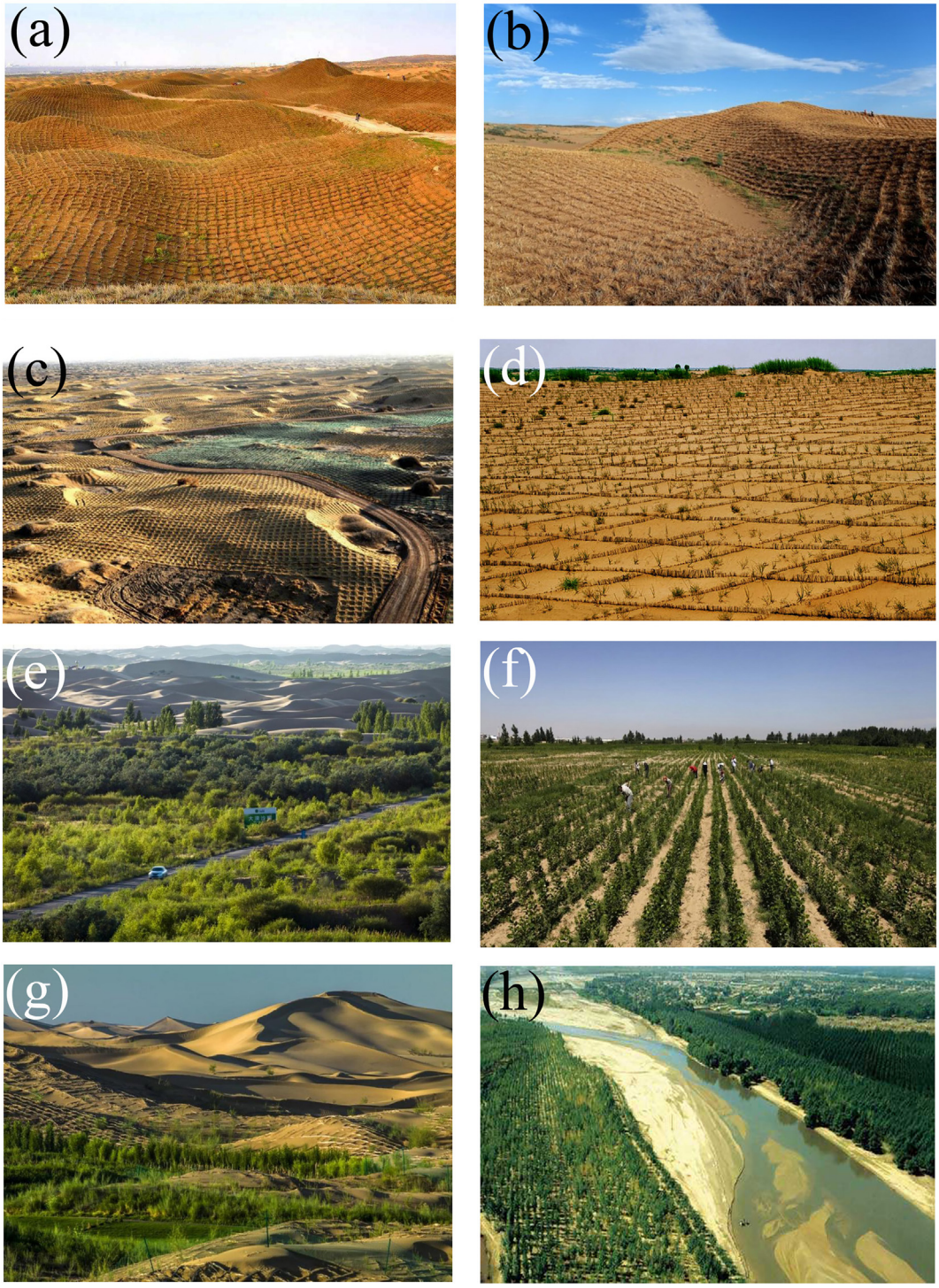

Fig. 9. The typical desertification prevention and control projects including grass pane and afforestation (photos from internet resources).

precipitation showed point clouds with relatively obvious informative boundaries, and the segmented quantile regression lines at pixel scale presented the exponential curves. The coefficients of determination (R^2) for fitted lines between wind erosion modulus and precipitation on the level of sub-zones in the NAR (i.e., Xinjiang, Gansu, and Inner Mongolia) were larger than 0.82. On the wind erosion modulus versus precipitation (Fig. 10(a–c)), the wind erosion modulus decreased exponentially with increasing precipitation. When precipitation increased from 50 to 150 mm yr^{-1}, the maximum soil loss decreased sharply from more than 500 to lower than 400 t ha^{-1} yr^{-1}; when precipitation increased from 150 to 250 mm yr^{-1}, soil loss decreased by another half; and when precipitation reached about 300 mm yr^{-1}, wind erosion was essentially stable (very slight). A possible explanation for this phenomenon (i.e., threshold effect of precipitation) is as follow: the area has sufficient precipitation and is commonly characterized by having a good vegetation cover and strong productivity, which can also effectively reduce soil loss induced by wind erosion. When precipitation is below the threshold (approximately 50 mm in Fig. 10(a–c)), the amount of precipitation (i.e., the water condition) is not sufficient to maintain a good vegetation cover; therefore, the vegetation is unable to efficiently prevent soil erosion. However, once the precipitation exceeds the threshold, the vegetation's soil retention function is enhanced and soil

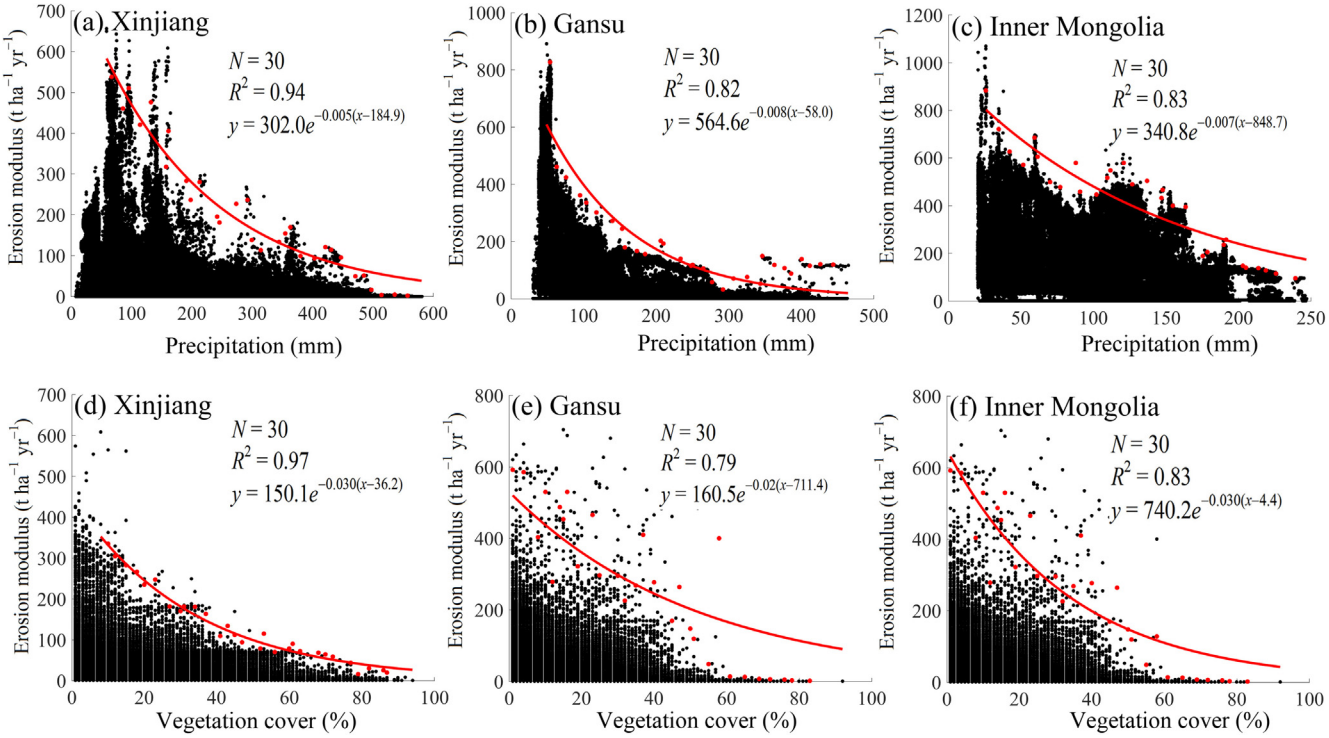

Fig. 10. Scatter plots (black dots), boundary points (red dots), and constraint lines (red lines) of (a–c) soil erosion modulus versus precipitation and (d–f) soil erosion modulus versus vegetation cover on the level of sub-zones in the NAG in 2010. (For interpretation of the references to colour in this figure legend, the reader is referred to the web version of this article.)

loss is substantially reduced.

4.5. Relationship between vegetation cover and wind erosion

Vegetation has long been recognized as a key factor in protecting soils from erosion through increasing surface roughness and absorbing the downward momentum of the ambient air stream (Wasson and Nanninga, 1986; Li et al., 2005). The below-ground parts of vegetation can not only enhance the stability of soil mass, but also reduce the scouring influences of runoff. Meanwhile, the above-ground parts of the plant can decrease the erosive force of precipitation (Shi et al., 2002). Therefore, the influences of vegetation cover on soil erosion are analyzed. In the Fig. 10(d–f), the scatter plots of soil erosion modulus against vegetation cover showed point clouds with relatively obvious informative boundaries, and both the segmented quantile regression lines at pixel scale presented exponential curves. The coefficients of determination (R^2) for fitted lines between wind erosion modulus and vegetation cover on the level of three sub-zones in the NAR were bigger than 0.79 (Fig. 10(d–f)). For the wind erosion modulus versus vegetation cover, the maximum wind erosion modulus decreased exponentially with increasing vegetation cover (Fig. 10(d–f)). When vegetation cover increased from 10 to 20%, the maximum soil loss decreased sharply from more than 400 to lower than 300 $t\,ha^{-1}\,yr^{-1}$; when vegetation cover increased from 20 to 40%, soil loss decreased by another half; and when vegetation cover reached over 40%, wind erosion was essentially stable (very slight).

Previous studies reported that the soil erosion modulus decreased exponentially with increasing vegetation cover (Lancaster and Baas, 1998; Yan et al., 2011), suggesting a strong correlation between the two variables. Our results also indicate that vegetation cover has a nonlinear constraint effect on soil erosion, meaning that vegetation acts as a limiting factor to wind erosion that is influenced simultaneously by multiple factors. Thus, vegetation cover alone cannot predict the actual amount of soil loss without considering other key factors. This study clearly indicates a constraint line that approximates the maximum soil loss with changing vegetation cover. Our results suggested that vegetation cover had a lower and an upper threshold for controlling wind erosion in the NAR, and the maximum soil loss declined precipitously with increasing vegetation cover between these two threshold values (Fig. 10(d–f)). Specifically, the lower threshold of vegetation cover was about 10%, below which vegetation had little effect on soil erosion. This suggested that plant cover lower than 10% did little to reduce wind velocity at the soil surface. The upper threshold was about 40%, beyond which soil erosion was essentially stable (very slight), implying that the effect of vegetation on reducing wind erosion basically reached the maximum when plant cover was 40% or above. However, a better understanding of this phenomenon requires field-based observational and experimental studies in the future.

4.6. Implications of the constraint effect in soil erosion control

In order to control soil erosion, the government has initialed a series of desertification prevention and control programs (e.g., GGWP, GFGP, and the Beijing–Tianjin Sandstorm Source Control Project). However, in many areas of northern China, their efficiency or cost–benefit ratio can certainly be improved (e.g., Zhang et al., 2014; Hu et al., 2015; Wu et al., 2015). In the arid and semiarid areas, water availability is the most important constraint factor for maintaining vegetation growth and further to control soil erosion. If planted vegetation cover is too high, the costs can be prohibitive. If the cover is too low, the vegetation does little to control soil erosion. As the specific guide in the NAR (i.e., Xinjiang, Gansu, and Inner Mongolia), our study suggests that vegetation cover should be at least higher than 10%, but there is no need to exceed 40% when planting vegetation to reduce wind erosion. In the NAR, the limited precipitation cannot support large areas of trees in a long term if human disturbances are removed (Wu et al., 2015; Feng et al., 2016), thus the constraint effects of water condition (precipitation) on vegetation cover should be considered to improve the efficiency of afforestation and reforestation efforts. Our study provides an important support for desertification prevention and control on local

and regional scales. However, the optimal vegetation cover varies from place to place, and it should be determined locally by considering other factors such as climate condition, soil type, topography, vegetation species, and their spatial patterns.

5. Uncertainties and limitations

Overall, although the model estimated soil erosion was validated according to literature derived data, there were still considerable uncertainties in the model's input parameters. The most reliable data of soil erosion come from field monitoring, but unfortunately not too many data are available. Therefore, the emphasis of future studies should be placed on improving the accuracy and robustness of biophysical models. In addition, more and more high-resolution remote sensing data of vegetation, soil, topography, and other biophysical factors are expected to provide sufficient independent data sources for soil erosion estimation, and to help calibrate and validate wind erosion models. Secondly, soil loss and sand retention were estimated using the RWEQ, which the input parameters (i.e., climatic factors and vegetation cover) had the problems of variable interdependence or circular reasoning. Finally, our statistical analyses on the effects of climate and vegetation cover on soil erosion suggest the possible mechanisms behind the effects although correlation is not causation. Field-based and process-oriented studies are still needed to verify these effects and understand the underlying mechanisms. Our study about the threshold of vegetation cover provides an important support for ecological restoration on local and regional scales. However, the optimal vegetation cover varies from place to place, and it should be determined locally by considering other factors such as climate condition, soil type, topography, vegetation species, and their spatial patterns.

6. Conclusions

In this study, the spatio-temporal change of wind erosion was identified, and the underlying drivers of soil erosion process were investigated. In addition, the implications of constraint effects in soil erosion control were discussed. In the NAR, both land cover type and soil property contributed to the spatial pattern of wind erosion significantly. The wind erosion processes usually occur in desert and sandy land with arid climate and low vegetation cover. The wind erosion from 1990 to 2013 was substantially lessened largely, because both favorable changes in climate (i.e., increasing precipitation and declining wind speed) and governmental policies for desertification prevention and control promoted vegetation restoration and expansion, thus resulting in a generally decreasing trend in soil erosion. The constraint line analyses indicate that the vegetation cover has nonlinear and threshold effects on soil erosion through constraining the water condition (precipitation). In the NAR, if the precipitation is below approximately 50–100 mm yr^{-1}, which means the precipitation (water condition) is not sufficient to maintain a good vegetation cover (about 20–40%), the vegetation cannot efficiently prevent wind erosion. However, once the precipitation exceeds the threshold, the vegetation's sand retention function will enhance and thus reducing soil loss substantially. Vegetation cover has a lower and an upper threshold for controlling wind erosion. This suggests that plant cover lower than 10% does little to reduce wind velocity at the soil surface. The upper threshold is about 40%, beyond which soil erosion is essentially stable, implying that the effect of vegetation on reducing wind erosion basically reaches the maximum when plant cover is 40% or above. In the NAR, the limited precipitation cannot support large areas of trees in a long-term if human disturbances are removed, thus the constraint effects of water condition (precipitation) on vegetation cover should be considered to improve the efficiency of afforestation and reforestation efforts.

Acknowledgements

This study is jointly funded by National Natural Science Foundation of China (NSFC) (No. 41625001; 4157A22) and the Strategic Priority Research Program of Chinese Academy of Sciences (No. XDA 20060402). Additional support was provided by the Southern University of Science and Technology (SUSTech; No. G01296001) and the Presidential Postdoctoral Fellowship. The authors would like to thank the two anonymous reviewers for their helpful and constructive comments and suggestions which have substantially improved the quality of this manuscript.

Appendix A. Supplementary data

Supplementary data to this article can be found online at https://doi.org/10.1016/j.ecoleng.2018.11.014.

References

Alexander, J.K., Philip, N.O., Ellen, L.P., David, A.L., 2017. The role of soil surface properties on the particle size and carbon selectivity of interrill erosion in agricultural landscapes. Catena 153, 194–206.
Ascough, J.C., Baffaut, C., Nearing, M.A., Liu, B., 1997. The WEPP watershed model: I Hydrology and erosion. Trans. ASAE 40 (4), 921–933.
Baigorria, G.A., Romero, C.C., 2007. Assessment of erosion hotspots in a watershed: integrating the WEPP model and GIS in a case study in the Peruvian Andes. Environ. Model. Softw. 22, 1175–1183.
Bourke, M.C., Pickup, G., 1999. Fluvial form variability in arid central Australia. In: Miller, A.J., Gupta, A. (Eds.), Varieties of Fluvial Form. Wiley, Chichester, pp. 249–271.
Bullard, J.E., McTainsh, G.H., 2003. Aeolian-fluvial interaction in dryland environments: example, concept and Australia case study. Proc. Phys. Geogr. 27, 471–501.
Cantón, A., Solé-Benet, J., De Vente, C., Boix-Fayos, A., Calvo Cases, C., Asensio, J., 2011. A review of runoff generation and soil erosion across scales in semiarid southeastern Spain. J. Arid Environ. 75, 1254–1261.
Coen, G.M., Tatarko, J., Martin, T.C., Cannon, K.R., Goddard, T.W., Sweetland, N.J., 2004. A method for using WEPS to map wind erosion risk of Alberta soils. Environ. Model. Softw. 19 (2), 185–189.
Du, H., Xue, X., Wang, T., 2014a. Estimation of the quantity of aeolian saltation sediments blown into the Yellow River from the Ulanbuh Desert, China. J. Arid Land 6 (2), 205–218.
Du, H., Xue, X., Wang, T., 2014b. Estimation of saltation emission in the Kubuqi Desert, North China. Sci. Total Environ. 479–480, 77–92.
Du, H., Xue, X., Wang, T., Deng, X., 2015. Assessment of the wind erosion risk in the watershed of the Ningxia-Inner Mongolia reach of the Yellow River, northern China. Aeolian Res. 17, 193–204.
Du, H., Dou, S., Deng, X., Xue, X., Wang, T., 2016. Assessment of wind and water erosion risk in the watershed of the Ningxia-Inner Mongolia Reach of the Yellow River, China. Ecol. Indic. 67, 117–131.
Duan, H., Yan, C., Tsunekawa, A., Song, X., Li, S., Xie, J., 2011. Assessing vegetation dynamics in the Three-North Shelter Forest region of China using AVHRR NDVI data. Environ. Earth Sci. 64, 1011–1020.
Fang, J., Chen, A., Peng, C., Zhao, S., Ci, L., 2001. Changes in forest biomass carbon storage in China between 1949 and 1998. Science 292, 2320–2322.
Feng, X., Fu, B., Piao, S., Wang, S., Philippe, C., Zeng, Z., Lü, Y., Zeng, Y., Li, Y., Jiang, X., Wu, B., 2016. Revegetation in China's Loess Plateau is approaching sustainable water resource limits. Nat. Clim. Change 6 (11), 1019–1022.
Feng, Z., Zhang, P., Yang, Y., 2003. The scale of land conversion from farmland to forest or grassland, the grain response to it, and the relevant proposals in Northwest China. Geogr. Res. 22 (1), 105–113.
Fryrear, D.W., Saleh, A., Bilbro, J.D., Schomberg, H.M., Stout, J.E., Zobeck, T.M., 1998. Revised Wind Erosion Equation. USDA, ARS, Technical Bulletin No. 1, June 1998.
Ganasri, B.P., Ramesh, H., 2016. Assessment of soil erosion by RUSLE model using remote sensing and GIS - a case study of Nethravathi Basin. Geosci. Front. 7, 953–961.
Gong, G., Liu, J., Shao, Q., 2014a. Wind erosion in Xilingol League, Inner Mongolia since the 1990s using the Revised Wind Erosion Equation. Process. Geogr. 33, 825–834.
Gong, G., Liu, J., Shao, Q., 2014b. Effects of vegetation coverage change on soil conservation service of typical steppe in Inner Mongolia. Geo-Inf. Sci. 16 (3), 426–434.
Gong, G., Liu, J., Shao, Q., Zhai, J., 2014c. Sand-fixing function under the change of vegetation coverage in a wind erosion area in northern China. J. Resour. Ecol. 5 (2), 105–114.
Guo, Q., Brown, J.H., Enquist, B.J., 1998. Using constraint lines to characterize plant performance. Oikos 83, 237–245.
Guo, B., Tao, H., Liu, B., Jiang, L., 2012. Characteristics and analysis of soil erosion in Li country after Wenchuan earthquake based on GIS and USLE. Trans. CSAE 28, 118–126.
Guo, B., Yang, G., Zhang, F., Han, F., Liu, C., 2018. Dynamic monitoring of soil erosion in the upper Minjiang Catchment using an improved soil loss equation based on remote sensing and geographic information system. Land Degrad. Dev. https://doi.org/10.1002/ldr.2882.

Hagen, L.J., 2004. Evaluation of the Wind Erosion Prediction System (WEPS) erosion submodel on cropland fields. Environ. Model. Softw. 19, 171–176.
Hao, R., Yu, D., Wu, J., 2017. Relationship between paired ecosystem services in the grassland and agro-pastoral transitional zone of China using the constraint line method. Agric. Ecosyst. Environ. 240, 171–181.
He, B., Chen, A., Wang, H., Wang, Q., 2015. Dynamic response of satellite-derived vegetation growth to climate change in the Three North Shelter Forest Region in China. Remote Sens. 7, 9998–10016.
Hoffmann, C., Funk, R., Reiche, M., Li, Y., 2011. Assessment of extreme wind erosion and its impacts in Inner Mongolia, China. Aeolian Res. 3, 343–351.
Hu, H., Fu, B., Lu, Y., Zheng, Z., 2015. SAORES: a spatially explicit assessment and optimization tool for regional ecosystem services. Landscape Ecol. 30, 547–560.
Jiang, L., Bian, J., Li, A., Lei, G., Nan, X., Feng, W., Li, G., 2014. Spatial-temporal changes of soil erosion in the upper reaches of Minjiang River from 2000 to 2010. J. Soil Water Conserv. 28, 19–25.
Jiang, C., Zhang, H., Tang, Z., Lev, L., 2017. Evaluating the coupling effects of climate variability and vegetation restoration on ecosystems of the Loess Plateau, China. Land Use Policy 69, 134–148.
Jones, L.S., Blakey, R.C., 1997. Eolian-fluvia interaction in the Page Sandstone (Middle Jurassic) in south-central Utah, USA – a case study of erg-margin processes. Sediment. Geol. 109, 181–198.
Knighton, A.D., Nanson, G.G., 1994. Waterholes and their significance in the anastomosing channel system of Cooper Creek, Australia. Geomorphology 9, 311–324.
Knisel, W.G., 1980. CREAMS: a field scale model for Chemicals, Runoff, and Erosion from Agricultural Management Systems. Washington D.C., Conservation Research Report, USDA, 26, 44.
Lancaster, N., Baas, A., 1998. Influence of vegetation cover on sand transport by wind: field studies at Owens Lake, California. Earth Surf. Proc. Land 23, 69–82.
Li, F., Kang, L., Zhang, H., Zhao, L., Shirato, Y., Taniyama, I., 2005. Changes in intensity of wind erosion at different stages of degradation development in grasslands of Inner Mongolia, China. J. Arid Environ. 62, 567–585.
Li, Z., Liu, C., Dong, Y., Chang, X., Nie, X., Liu, L., Xiao, H., Lu, Y., Zeng, G., 2017. Response of soil organic carbon and nitrogen stocks to soil erosion and land use types in the Loess hilly–gully region of China. Soil Tillage Res. 166, 1–9.
Liu, J., Liu, M., Tian, H., Zhuang, D., Zhang, Z., Zhang, W., Tang, X., Deng, X., 2005. Spatial and temporal patterns of China's cropland during 1990–2000: an analysis based on Landsat TM data. Remote Sens. Environ. 98, 442–456.
Liu, J., Kuang, W., Zhang, Z., Xu, X., Qin, Y., Ning, J., Zhou, W., Zhang, S., Li, R., Yan, C., Wu, S., Shi, X., Jiang, N., Yu, D., Pan, X., Chi, W., 2014. Spatio-temporal characteristics, patterns and causes of land-use changes in China since the late 1980s. J. Geogr. Sci. 24 (2), 195–210.
Liu, L., Wang, J., Li, X., Liu, Y., Ta, W., Peng, H., 1998. Wind tunnel measured for wind erodible sand particles of arable lands. Chin. Sci. Bull. 43, 1163–1166.
Mattheus, C.R., Norton, M.S., 2015. Comparison of pond-sedimentation data with a GIS-based USLE model of sediment yield for a small forested urban watershed. Anthropocene 2, 89–101.
McIntosh, R.J., 1983. Floodplain geomorphology and human occupation of the upper inland delta of the Niger. Geogr. J. 149, 182–201.
Mckenna Neuman, C., 2003. Effects of temperature and humidity upon the entrainment of sedimentary particles by wind. Bound-Layer Meteorol. 108 (1), 61–89.
Mendez, M.J., Buschiazzo, D.E., 2010. Wind erosion risk in agricultural soil under different tillage systems in the semiarid Pampas of Argentina. Soil Tillage Res. 106, 311–316.
Ministry of Water Resources of the People's Republic of China (MWRPRC), 2001. The Second National Remote Sensing Survey of Soil Loss.
Morgan, R.P.C., Quinton, J.N., Smith, R.E., Govers, G., Poesen, J.W.A., Auerswald, K., Chisci, G., Torri, D., Styczen, M.E., 1998. The European Soil Erosion Model (EUROSEM): a dynamic approach for predicting sediment transport from fields and small catchments. Earth Surf. Process. Landforms 23, 527–544.
Naser, K., Mehdi, S., Hossein, A., Manuchehr, G., Masoud, D., 2016. Modeling soil loss at plot scale with EUROSEM and RUSLE2 at stony soils of Khamesan watershed, Iran. Catena 147, 773–788.
Parungo, F., Li, Z., Li, X., Yang, D., Harris, J., 1994. Gobi dust storms and The GreatGreen Wall. Geophys. Res. Lett. 21 (11), 999–1002.
Pimental, D., Harvey, C., Resosudarmo, P., 1995. Environmental and economic costs of soil erosion and conservation benefits. Science 267, 111741123.
Qu, B., Zhu, W., Jia, S., Lv, A., 2015. Spatio-temporal changes in vegetation activity and its driving factors during the growing season in china from 1982 to 2011. Remote Sens. 7, 13729–13752.
Renard, K.G., Foster, G.R., Weesies, G.A., McCool, D.K., Yoder, D.C., 1997. Predicting Soil Erosion by Water: A Guide to Conservation Planning with the Revised Universal Soil Loss Equation (RUSLE) Handbook No. 703. US Department Agriculture, 404.
Rezaei, M., Sameni, A., Shamsi, S.R.F., Bartholomeus, H., 2016. Remote sensing of land use/cover changes and its effect on wind erosion potential in southern Iran. Peerj. https://doi.org/10.7717/peerj.1948.
Samani, Z.A., Pessarakli, M., 1986. Estimating potential crop evapotranspiration with minimum data in Arizona. Trans. Am. Soc. Agric. Eng. 29 (2), 522–524.
Shao, Y., 2008. Physics and Modelling of Wind Erosion. Springer, New York.
Shi, Z., Cai, C., Ding, S., Li, C., Wang, T., 2002. Soil conservation planning at small watershed level using GIS based revised universal soil loss equation (RUSLE). Trans. CSAE 18, 172–175.
Singer, M.J., Warkentin, B.P., 1996. Soils in an environmental context: an American perspective. Catena 27, 179–189.
Skidmore, E.L., Tatarko, J., 1990. Stochastic wind simulation for erosion modeling. Trans. ASAE 33 (6), 1893–1899.
Song, Z., 2004. A numerical simulation of dust storms in China. Environ. Model. Softw. 9, 141–151.
State Forestry Administration (SFA), 2010. Plan for the Desertification Prevention and Control Project Around the Tarim Basin, Xinjiang Uygur Autonomous Region (2011–2015). State Forestry Administration.
Tamene, L., Parl, S.G., Dikau, R., Vlek, P.L.G., 2006. Analysis of factors determining sediment yield variability in the highlands of Northern Ethiopia. Geomorphology 76, 76–91.
Tan, M., Li, X., 2015. Does the Green Great Wall effectively decrease dust storm intensity in China? A study based on NOAANDVI and weather station data. Land Use Policy 43, 42–47.
Tang, K., 2004. Soil and Water Conservation in China. Chinese Science Press, Beijing.
Tang, B., Jiao, J., Yan, F., Li, H., 2018. Variations in soil infiltration capacity after vegetation restoration in the hilly and gully regions of the Loess Plateau, China. J. Soils Sediments. https://doi.org/10.1007/s11368-018-2121-1.
Teller, J.T., Lancaster, N., 1986. Lacustrine sediments at Narabeb in the central Namib Desert, Namibia. Palaeogeogr. Palaeoclimatol. Palaeoecol. 56, 177–195.
Thomson, J.D., Weiblen, G., Thomson, B.A., Alfaro, S., Legendre, P., 1996. Untangling multiple factors in spatial distributions lilies, gophers, and rocks. Ecology 77, 1698–1715.
Vanwalleghem, T., Gómez, J.A., Infante, J.A., Molina, M.G.D., Vanderlinden, K., Guzmán, G., Laguna, A., Giráldez, J.V., 2017. Amate Impact of historical land use and soil management change on soil erosion and agricultural sustainability during the Anthropocene. Anthropocene 17, 13–29.
Walling, D., He, Q., Whelan, P., 2003. Using 137Cs measurements to validate the application of the AGNPS and ANSWERS erosion and sediment yield models in two small Devon catchments. Soil Tillage Res. 69, 27–43.
Wang, T., Feng, L., Mou, P., Wu, J., Smith, J.L., Xiao, W., Yang, H., Dou, H., Zhao, X., Cheng, Y., 2016a. Amur tigers and leopards returning to China: direct evidence and a landscape conservation plan. Landscape Ecol. 31, 491–503.
Wang, X., Lu, C., Fang, J., Shen, Y., 2007. Implications for development of grain-for-green policy based on cropland suitability evaluation in desertification affected north China. Land Use Policy 24, 417–424.
Wang, X., Zhang, C., Hasi, E., Dong, Z., 2010. Has the Three Norths Forest Shelterbelt Program solved the desertification and dust storm problems in arid and semiarid China? J. Arid Environ. 74, 13–22.
Wang, X., Zhao, X., Zhang, Z., Li, Y., Zuo, L., Wen, Q., Liu, F., Xu, J., Hu, S., Liu, B., 2016b. Assessment of soil erosion change and its relationships with land use/cover change in China from the end of the 1980s to 2010. Catena 137, 256–268.
Wasson, R., Nanninga, P., 1986. Estimating wind transport of sand on vegetated surfaces. Earth Surf. Proc. Land. 11, 505–514.
Wei, S., Zhang, X., McLaughlin, N., Chen, X., Jia, S., Liang, A., 2017. Impact of soil water erosion processes on catchment export of soil aggregates and associated SOC. Geoderma 294, 63–69.
Wu, J., Zhang, Q., Li, A., Liang, C., 2015. Historical landscape dynamics of Inner Mongolia: patterns, drivers, and impacts. Landscape Ecol. 30, 1579–1598.
Xiao, Q., Hu, D., Xiao, Y., 2017. Assessing changes in soil conservation ecosystem services and causal factors in the Three Gorges Reservoir region of China. J. Clean. Prod. 163, S172–S180.
Xu, L., Xu, Y., Meng, X., 2013. Risk assessment of soil erosion in different rainfall scenarios by RUSLE model coupled with Information Diffusion Model: a case study of Bohai Rim, China. Catena 100, 74–82.
Yan, Y., Xu, X., Xin, X., Yang, G., Wang, X., Yan, R., Chen, B., 2011. Effect of vegetation coverage on aeolian dust accumulation in a semiarid steppe of northern China. Catena 87, 351–356.
Yin, R., Yin, G., 2010. China's primary programs of terrestrial ecosystem restoration: initiation, implementation, and challenges. Environ. Manage. 45, 429–441.
Youssef, F., Visser, S., Karssenberg, D., Bruggeman, A., Erpul, G., 2012. Calibration of RWEQ in a patchy landscape: a first step towards a regional scale wind erosion model. Aeolian Res. 3, 467–476.
Zhang, J., Niu, J., Buyantuev, A., Wu, J., 2014. A multilevel analysis of effects of land use policy on land-cover change and local land use decisions. J. Arid Environ. 108, 19–28.
Zhang, Y., Peng, C., Li, W., Tian, L., Zhu, Q., Chen, H., Fang, X., Zhang, G., Liu, G., Mu, X., Li, Z., Li, S., Yang, Y., Wang, J., Xiao, X., 2016. Multiple afforestation programs accelerate the greenness in the 'Three North' region of China from 1982 to 2013. Ecol. Indic. 61, 404–412.
Zhang, P., Shao, G., Zhao, G., Master, D.C.L., Parker Jr., G.R., Dunning, J.B., Li, Q., 2000. China's forest policy for the 21st century. Science 288, 2135–2136.
Zhang, Y., Wei, L., Wei, X., Liu, X., Shao, M., 2018. Long-term afforestation significantly improves the fertility of abandoned farmland along soil clay gradient on the Chinese Loess Plateau. Land Degrad. Dev. https://doi.org/10.1002/ldr.3126.
Zhao, G., Mu, X., Wen, Z., Wang, F., Gao, P., 2013. Soil erosion, conservation, and eco-environment changes in the loess plateau of China. Land Degrad. Dev. 24, 499–510.
Zhao, G., Tian, P., Mu, X., Jiao, J., Wang, F., Gao, P., 2014. Quantifying the impact of climate variability and human activities on streamflow in the middle reaches of the Yellow River basin, China. J. Hydrol. 519, 387–398.
Zhao, G., Mu, X., Jiao, J., An, Z., Klik, A., Wang, F., Jiao, F., Yue, X., Gao, P., Sun, W., 2017. Evidence and caused of spatial temporal changes in runoff and sediment yield on the Chinese Loess Plateau. Land Degrad. Dev. 28, 579–590.
Zhou, J., Fu, B., Gao, G., Lü, Y., Liu, Y., Lu, N., Wang, S., 2016. Effects of precipitation and restoration vegetation on soil erosion in a semi-arid environment in the Loess Plateau, China. Catena 137, 1–11.
Zhu, J., Zhou, X., Hu, J., 2004. Thoughts and views about the three north shelterbelt program. J. Nat. Res. 19 (1), 79–85.